Ultramicroscopy 000 (2017) 1–11

Contents lists available at ScienceDirect

Ultramicroscopy

journal homepage: www.elsevier.com/locate/ultramic

Vibrational and valence aloof beam EELS: A potential tool for nondestructive characterization of nanoparticle surfaces

Peter A. Crozier

Materials Program, School for the Engineering of Matter, Transport and Energy, Arizona State University, 501 E. Tyler Mall, Tempe, AZ 85287-6106, USA.

ARTICLE INFO

Article history:
Received 8 November 2016
Revised 10 March 2017
Accepted 11 March 2017
Available online xxx

Keywords:
Electron energy-loss spectroscopyp
EELS
Surface analysis
Catalysts
Ondrej Krivanek

ABSTRACT

In many materials systems, electron beam effects may substantially alter and destroy the structure of interest during observation. This is often true for the surface structures of catalytic nanoparticles where the functionality is associated with thin surface layers which are easily destroyed. The potential application of using aloof beam electron energy-loss spectroscopy as a non-destructive nanoscale surface characterization tool is discussed. Recent developments in monochromators make vibration and valence loss EELS possible in the electron microscope. The delocalization associated with these signals allows spectra to be acquired when the electron beam is position 2 nm or more away from the particle surface. This eliminates knock-on damage and significantly reduces ionization damage. Theoretical and experimental results are employed to explore the potential strengths and weaknesses of monochromated aloof beam EELS for surface analysis. The approach is most favored for surface layers on insulators because the bandgap lowers the background for detection of the vibrational signal and bandgap states. Guided light modes and relativistic effects can complicate the interpretation of the spectra. The effects are suppressed at lower accelerating voltages and particle size especially for low refractive index materials.

1. Introduction

Electron energy-loss spectroscopy (EELS) in the (scanning) transmission electron microscope (STEM/TEM) is a vital tool for performing high spatial resolution analysis of composition, bonding and optical properties in materials. The development of aberration correction has pushed the spatial resolution of STEM to below 1 Å allowing composition and electronic structure to be probed down to the atomic level at interfaces, grain boundaries as well as exploring variations present in nanoparticles. In parallel with these improvements in spatial resolution, spectral energy resolution has also improved revealing finer detail in electronic structure. However, for many applications, electron beam effects substantially alter the structure during observation. This is often true for the surface structures of catalytic nanoparticles where the functionality is associated with thin surface layers which are easily destroyed. These surface structures form only under reaction conditions and lie at the heart of our attempts to understand structure-function relations. To observe and characterize these structures in the TEM, *in situ* observations at elevated temperatures and pressures may be necessary using techniques such as environmental TEM (ETEM) [1–3]. It would be ideal to develop non-destructive nanoscale spectroscopic tools which could be performed under *operando* conditions. Optical vibrational spectroscopy is often employed to identify surface adsorbates on catalyst surfaces. Indeed, the first use of the term "*operando*" was coined for *in situ* Raman spectroscopy of catalysts in their working states [4]. It may now be possible to obtain similar information from the TEM using aloof beam vibrational and valence loss EELS. Ondrej Krivanek and others have played a key role in the instrumentation improvements which enable the nanoparticle surface analysis question to now be seriously considered. The first few sections of this paper describe some of the historical developments leading to high energy resolution valence and vibrational EELS in the STEM including the critical role that Ondrej played. Sections 5–8 of this manuscript consider some of the fundamental questions associated with using aloof beam EELS to perform nondestructive probing of nanoparticle surfaces.

The early generation of dedicated STEMs, pioneered initially by Crewe and then commercialized by VG Microscopes, used cold field emission electron guns (FEG) [5]. In addition to high brightness allowing small intense probe formation, the cold FEG had much smaller energy spread than thermal electron sources offering the potential of energy resolutions approaching 250 meV. Although early spectrometers and electronic stability were limited, initial STEM EELS on nucleic acids demonstrated that high energy resolution EELS contained a wealth of sample information [6,7]. Isaacson published a series of papers in EELS and outlined the value of EELS for light element analysis [8].

E-mail address: crozier@asu.edu

http://dx.doi.org/10.1016/j.ultramic.2017.03.011
0304-3991/

Around the same time, a talented young student named Ondrej Krivanek was finishing a Ph.D. at Cambridge under the mentorship of Prof. Archie Howie. Ondrej had just published a series of important papers on TEM image formation processes [9–11]. After Cambridge he worked briefly at the University of Kyoto and obtained the first atomic resolution images of grain boundaries in germanium [12]. In 1978, he attended a workshop at Cornell and developed an interest in EELS. Ondrej's long association with Arizona State University (ASU) started a few years later in 1980 when he took a faculty position as Associate Director of the NSF Facility on High Resolution Electron Microscopy. His interest in spectroscopy continued to grow and develop tackling, for example, topics such as extended edge fine structure [13]. Ondrej was involved in many aspects of running the microscope facility and organized a workshop entitled "Imaging and Microanalysis with High Spatial Resolution" held at Castle Hot Springs just outside Phoenix in 1982 [14]. He also chaired the first of the ASU Winter Schools in High Resolution Electron Microscopy also in 1982. These schools have run almost continuously every January for 35 years (I have inherited the role as chair today). Ondrej designed his first spectrometer while at Berkeley and continued this project when he moved to ASU. Indeed, a critical publication, which does not appear in Web of Science or Google Scholar, presented at an EMAG/Metals Society meeting in Manchester, co-authored with the late Peter Swann of Gatan, shows a prototype compact magnetic prism design [15]. This spectrometer and its development ultimately resulted in Ondrej joining Gatan to commercialize this product and many other spectroscopy and imaging tools.

Ondrej's efforts at Gatan made spectrometers widely available and EELS became a common materials characterization tool in TEM. He continued to develop and commercialize instrumentation for EELS such as the use of photodiode arrays that allowed simultaneous measurement of 1000 energy-loss channels in the spectrum [16]. This was followed by his development and commercialization of the imaging filter in which additional electron optical elements were added after the magnetic prism to allow energy-filtered images or diffraction patterns to be acquired [17]. Ondrej remained engaged in educational activities and initiated a series of EELS schools at Gatan which continue to this day. At Lake Tahoe in August of 1990, he initiated the first in a series of workshops dealing with advanced developments in EELS and related areas. These meetings, known by the name EDGE (Enhanced Data Generated by Electrons), are held every four years at different locations around the world bringing together a small group of experts (in format similar to Gordon conferences) on novel developments, directions and applications for EELS. Ondrej chaired the first meeting and once again I inherited this task and served as scientific co-chair (with Gianluigi Botton) for the 2013 EDGE meeting in Sainte Maxime, France and will also co-chair (with Odile Stephan) the 2017 EDGE meeting in Okinawa, Japan.

2. Improvements in instrumentation leading to high energy and spatial resolution

Obtaining ultra-high energy resolution in the electron microscope was a result of steady improvements in electron sources, spectrometers and monochromators. Results from X-ray absorption spectroscopy at synchrotrons had shown there was a wealth of bonding information in the fine structure of ionization edges. It was recognized that similar information could potentially be obtained from STEM/TEM EELS, with high spatial resolution. The initial developments in this area came from groups working with dedicated STEMs because these instruments were already equipped with cold FEGs where the energy spread of the emitted electrons is around 300 meV resulting from the Fowler Nordheim distribution associated with the field emission process. Batson was the first to make improvements to the system stability of a dedicated STEM and using a Wien filter spectrometer achieved a system resolution of 250 meV [18]. Brydson and co-workers achieved 200 meV using an in-house system and acquired spectra from 3d transition metal oxides with 500 meV resolution [19,20]. Ondrej followed shortly after and demonstrated that his magnetic prism spectrometer coupled to a dedicated STEM could achieve resolutions of 300 meV allowing L_{23} edges from a variety of transition metal oxides to be acquired with energy resolution of 300–400 meV [21,22].

To obtain system resolutions much below 300 meV required the electron distribution leaving the source to be energy filtered using so-called monochromators. The goal of monochromation is to reduce the energy spread of electrons incident on the sample without significantly impacting spatial resolution and maintaining adequate electron beam current. Several TEM monochromators were developed in the 90 s based on Wien filters and electrostatic optical elements that resulted in resolutions of 100 meV [23–26]. These instruments were commercialized and once again the L_{23} edges of transition metal oxides were convenient test samples to demonstrate improved energy resolution [27]. Resolutions of around 100 meV are adequate to resolve features on inner-shell ionization edges where lifetime broadening gives intrinsic line widths of around 200 meV or greater [28]. Monochromators also opened up opportunities for exploring structures in the low-loss part of the spectrum including bandgap determination and exploration of plasmonic structures [29–36]. We employed monochromated EELS to investigate the optical properties of carbonaceous aerosols for climate modelling. The higher energy resolution and low zero-loss peak tails associated with monochromators allowed the complex refractive index to be determined across the entire energy range of interest to climate change from the near IR into the UV [37,38].

3. The Nion monochromator and Arizona State University

The existing monochromator systems were able to reveal a wealth of detail for core-loss EELS but were limited at energy-losses below 0.5 eV because of the very large background associated with the tails on the zero-loss peak arising from the detector modulation transfer function and the electron optics. This background reduces the detection limits for weak features such as states within the bandgap of semiconductors and insulators and is difficult to accurately model due to variations in zero-loss peak shape during acquisition. Moreover, it was recognized that further improvements in both energy resolution and instrumental background were required making detection of vibrational excitations possible with TEM EELS.

Ondrej had developed ideas for a monochromated system based on magnetic prisms in which electrons leaving the gun pass through an energy selecting slit while travelling along an alpha shaped trajectory [39]. Although alpha filters had been explored previously [40], the design proposed by Ondrej promised energy resolution down to 10 meV in a dedicated STEM. About the same time, Arizona State University electron microscopy group, under the leadership of Prof. Ray Carpenter, was lucky enough to secure funding from the US National Science Foundation and Arizona State University to purchase our first aberration corrected STEM. It was clear that the monochromator design proposed by Nion potentially represented a very large advance in terms of performance. Of course, there was no working prototype, all we had was the 2009 paper and assurances from Ondrej that he could make it work. Ondrej had an impressive track record on instrument developments such as the magnetic prism spectrometer, design, control and performance of imaging filters, as well as the aberration corrected STEM that Nion had successfully launched. The ASU group decided to order the first Nion monochromated STEM. In the original quote,

Please cite this article as: P.A. Crozier, Vibrational and valence aloof beam EELS: A potential tool for nondestructive characterization of nanoparticle surfaces, Ultramicroscopy (2017), http://dx.doi.org/10.1016/j.ultramic.2017.03.011

the target resolution was 30 meV, however, the preliminary results from the delivered instrument easily beat these specifications and we routinely run at 15–20 meV with beam sizes on the order of 0.5 nm or less [41].

4. Vibrational EELS and bandgap states

The excellent performance of the instrument motivated interest in the possibility of performing vibrational EELS in the STEM. Calculations of optical phonon scattering cross sections showed that their magnitude was similar to inner-shell ionization cross sections suggesting that characteristic losses associated with optical phonons should be detectable if the instrumental background was low enough [42,43]. Dr. Jiangtao Zhu, a postdoctoral fellow in my group, was trying to extend our determination of optical properties of aerosols deep into the IR. In some of the organic aerosols, we saw peaks at 300–400 meV that would be consistent with C–H and N–H vibrational excitations. Although these features were absent from graphitic aerosols, their appearance in the ambient organic aerosols was not consistent and peaks were also observed at 700 meV raising concerns about their interpretation. Factors such as radiation damage, instrumental artifacts and heterogeneity in sample composition all introduced complexity to the spectral interpretation. These results were presented at the 2013 Microscopy and Microanalysis conference in Indianapolis. In discussing the results with Ondrej, we decided that the best path forward was to have a collaboration between Nion, ASU and Rutgers to unambiguously look for vibrational modes during the fall of 2013.

Ondrej and the team from Nion made several trips to ASU to help in the hunt for phonons in the TEM. Vibrational signals from compounds containing hydrogen were initially considered to be the easiest test cases because of the relatively high energy loss involved i.e. 300–450 meV. After many long nights and many failures with a variety of hydrogen containing samples, the first unambiguous vibrational fingerprint was observed in hexagonal boron nitride (BN), the longitudinal optical phonon at ~170 meV [44]. For those of us in the EELS community, it was both fitting and amusing that the first detected phonons were in BN. For many years, hexagonal BN has been the definitive test sample for core-loss quantification procedures and near-edge fine structure. At ASU we often referred to it as "*boring nitride*" because we had seen the spectrum so many times. In hindsight, it was the perfect sample to use because it has a large bandgap and low refractive index of 1.8 suppressing relativistic effects and minimized the background on which the phonon signal sits. It is well behaved under the electron beam showing minimal charging and radiation damage. We went on and successfully detected vibrational peaks in other low refractive index materials such as the Si-O stretch mode in amorphous SiO_2 Stober spheres (see Fig. 1) and organics such as polymeric epoxy resin. Simultaneously, another group in Japan was also actively involved in pushing the resolution of monochromated systems. They achieved an energy resolution of 26 meV and observed vibrational excitations at about 400 meV associated with the C–H stretch modes in an ionic liquid [45]. Similar success has also been achieved with beautiful work from Phil Batson and Maureen Lagos at Rutgers on surface phonon modes on MgO cubes [46]. More recent exciting work on optical and acoustic phonons has been presented at the 2016 Microscopy and Microanalysis conference in Columbus by Quentin Rammasse and the SuperSTEM group at Daresbury.

The ability to locally detect electronic states within the bandgap region of the spectrum remains a considerable challenge in materials science. From an instrumental point of view, it is important not just to have high energy and spatial resolution but to have very low tails on the zero-loss peak so that weak features within the bandgap become more visible. Using the Nion monochromated system we have recently detected the presence of bandgap states associated with Pr solutes in CeO_2 [47]. Fig. 2 shows the background subtracted experimental spectra from pure CeO_2 and Pr doped CeO_2 with the latter showing an additional intensity plateau within the bandgap region with an onset energy of approximately 1.4 eV A relatively simple density of states approach was used to interpret the spectra allowing the approximate width and position of the bandgap state to be determined and in this case the result derived from monochromated EELS was in good agreement with optical methods. It is important to exercise some caution in the interpretation of spectral features within the bandgap. Effects such as cavity modes and Cherenkov radiation may also give rise to additional intensity in this region which may obscure the intensity associated with bandgap states (see Section 8).

5. Delocalization

The BN phonon intensity remains significant even when the electron beam is positioned 100 nm outside the sample. Classical and quantum mechanical treatments have been given and some of these are reviewed by Egerton [48]. The long range nature of the electromagnetic interaction of the fast electron with the sample has been treated by many authors and shows that, as the electron probe is scanned into the vacuum, the energy-loss signal falls fastest for high energy-losses and larger scattering angles. These treatments are consistent with the experimental observations of delocalization of vibrational EELS for the forward scattering case although some of the surface modes observed by Lagos et al appear to be localized to within a few nanometers [46].

The exact extent of delocalization for phonon losses remains a topic of ongoing theoretical and experimental research [49–52]. There are different mechanisms for excitation of vibrational modes with fast electron beams. Dipole scattering, where the field associated with the fast electron polarizes the medium, is generally believed to be responsible for a substantial fraction of the vibrational intensity observed in spectra recorded in the forward scattering direction. Classical dielectric theory is able to predict many of the experimentally observed spatial variations in the forwards scattered intensity for linescans into the vacuum and across Si/SiO_2 interfaces [53,54]. On the other hand, the atomic resolution high-angle annular dark-field imaging signal is associated with phonon scattering from small impact parameter events [55]. One may consider the vibrational signal to be composed of an intense low resolution contribution associated with low-angle scattering and a more localized component associated with higher-angle scattering. This is similar to the dipole and impact scattering regimes in low energy EELS for detecting surface vibrational states discussed by Ibach and others [56].

Achieving high spatial resolution vibrational spectroscopy remains an important goal for the electron microscopy community. The spatial resolution associated with the low-angle vibrational EELS is comparable with that obtained with near field optical methods which also report 10 s of nanometers spatial resolution [57–59]. For surface analysis of catalysts, these methods and techniques, such as scanning tunneling microscopy (STM), provide a powerful approach for determining surface layers and adsorbates with STM easily giving atomic resolution[1]. However, one advantage of TEM methods is that they can be applied to high surface area catalysts. Obtaining resolutions below 1 nm for vibrational EELS would be a major accomplishment. Theoretical calculations suggest that atomic resolution vibrational spectroscopy should be possible [49,51] and recent experimental work suggests a spatial resolution of around 1 nm in BN for the high angle scattered part of the vibrational signal [60]. In the meantime, a major advantage of performing vibrational spectroscopy in the STEM is the ability to correlate the spectroscopic signal with atomic resolution image

Please cite this article as: P.A. Crozier, Vibrational and valence aloof beam EELS: A potential tool for nondestructive characterization of nanoparticle surfaces, Ultramicroscopy (2017), http://dx.doi.org/10.1016/j.ultramic.2017.03.011

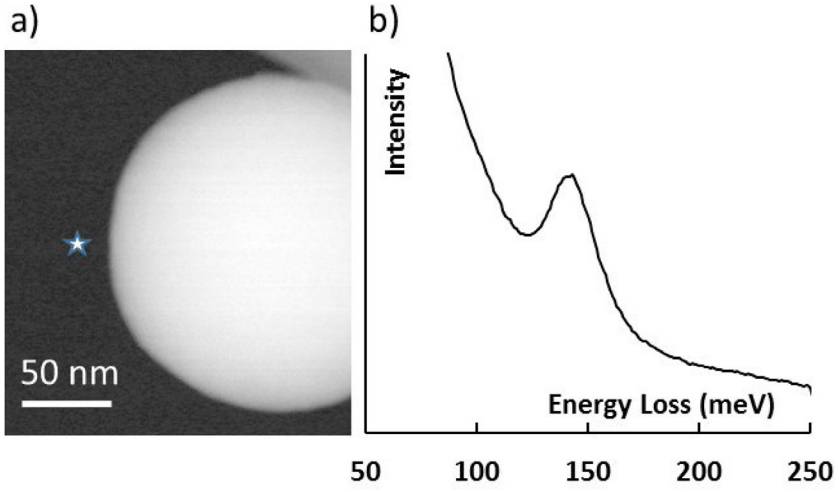

Fig. 1. a) Annular dark-field STEM image and **b)** vibrational EELS recorded at 100 kV from 200 nm amorphous SiO_2 Stober sphere, impact parameter b = 20 nm (indicated with star on image). The Si-O stretch mode is at 142 meV.

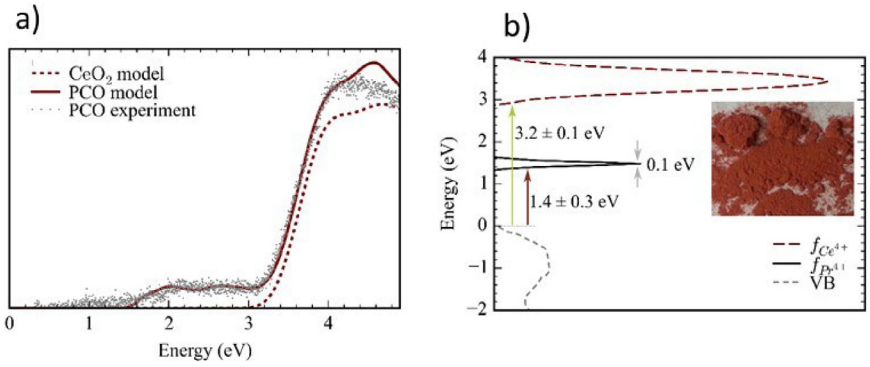

Fig. 2. a) Valence loss EELS recorded at 60 kV from CeO_2 and $Ce_{0.9}Pr_{0.1}O_{2-x}$ showing intensity within the bandgap associated with Pr 4f states. **b)** The density of states derived from the energy loss spectrum showing the position of the Pr state (black) between the CeO_2 valence (dotted grey) and conduction band (red). Insert shows $Ce_{0.9}Pr_{0.1}O_{2-x}$ powder after oxidation in air. (Courtesy Bowman et al [47], with permission Elsevier). (For interpretation of the references to colour in this figure legend, the reader is referred to the web version of this article.)

signals as well as valence and core loss spectra. For example, we have recently been able to correlate vibrational molecular fingerprints with bandgap measurements in carbon nitrides [61].

6. Aloof beam EELS

The delocalization of the forward scattered vibrational signal permits spectra to be acquired when the electron probe is positioned outside the sample. The idea of performing electron energy-loss spectroscopy with an electron beam that does not penetrate or get reflected from the surface seems to date back to work by Ballu and co-workers who were interested in surface plasmons on Mo [62,63]. These experiments were performed with electron energies of around 2000 eV and the authors applied an electric field to the sample to generate parabolic "nontouching trajectories". The advantage of this approach was that the spectral interpretation was simplified because the surface contribution was dominant. The first example of this approach being employed in a STEM was a conference paper on surface plasmons on Al spheres by Batson and Treacy [64]. This was followed by a series of papers from Batson et al on Al spheres and from Marks on MgO cubes [65–68]. Cowley also published STEM EELS results from MgO surfaces and interpreted the data in terms of channeling and transition radiation [69,70]. An example of an early so-called *aloof* beam spectrum from Al spheres is shown in Fig. 3. (The first use of the term "aloof beam" to describe energy-loss spectra when the beam does not pass through the sample dates to 1984 and work with 2000 eV electrons [71]).

The character of the aloof beam spectrum can be understood in terms of the dielectric function of the material and has been investigated mostly using classical electrodynamic models. If the dielectric function is known, the full numerical simulations of energy loss spectra can be performed for objects of arbitrary shape. Analytical expressions for non-relativistic and relativistic cases have also been derived for simple geometries such as planar interfaces or spheres. The simplest geometry is the so-called infinite half plane which assumes a flat interface between two materials with an electron beam moving through one medium parallel to the interface and a distance b from the interface. Relativistic and non-relativistic treatments have been given for this problem, for example [72–77]. If the medium through which the electron beam is travelling is the vacuum, then the spectral intensity, S(E), at energy-loss, E, can be related to the complex dielectric function, ε, impact parameter (the beam position from the sample surface) b, through the relationship

$$S(E) \propto K_o\left(\frac{2\omega b}{v}\right) Im\left[\frac{-1}{(\epsilon(E)+1)}\right]/v^2 \qquad (1)$$

with v the electron velocity, $E = \bar{h}\omega$, $\bar{h} = h/2\pi$ with h the Planck constant, and K_o is a zeroth order modified Bessel function. The Bessel function contains the spatial dependence of the signal as the beam is translated away from the surface with increasing impact

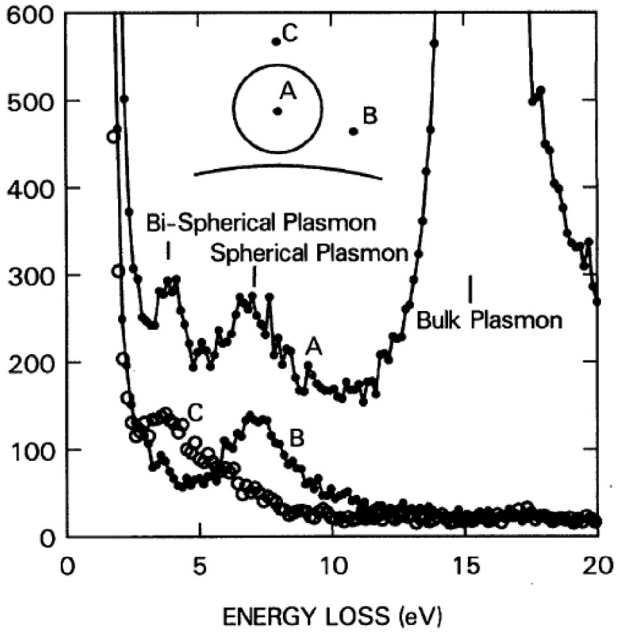

Fig. 3. Early example of aloof beam EELS from aluminum/alumina spheres. The position of the electron probe with respect to the 10 nm Al particle is shown in the insert. Spectra marked B and C are recorded from the beam outside the sample. The bulk plasmon signal is completely absent from the aloof spectrum and several different surface modes show up. (From Batson, [66] with permission APS).

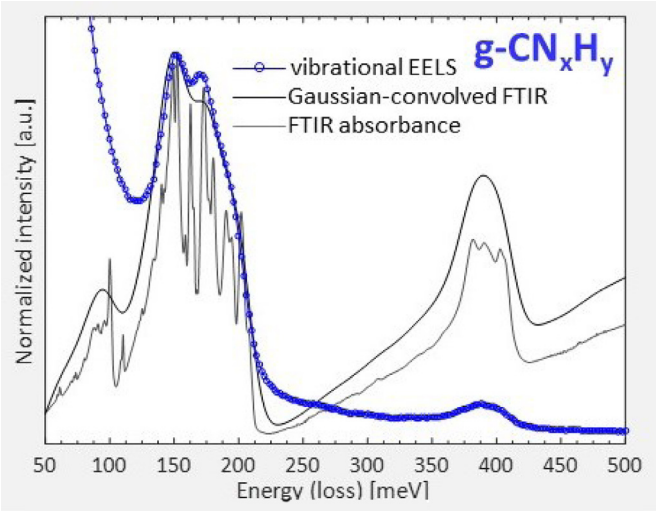

Fig. 4. Aloof beam vibrational EELS (blue) from g-CN_xH_y recorded at 60 kV. FTIR spectrum recorded from identical material and convolution of FTIR spectrum with response function correspond to energy resolution of EELS. (Courtesy Diane Haiber, Arizona State University). (For interpretation of the references to colour in this figure legend, the reader is referred to the web version of this article.)

parameter, b, i.e. this is the delocalization term. Similar expressions have also been derived for other simple geometries such as spheres and cylinders [73–75,78–80]. In general, ε can also depend on momentum transfer $\hbar q$ and the direction of the electric field but these other effects are often ignored. The infinite slab model seems to be qualitatively useful but is not always appropriate. It strictly applies only when the thickness t of the truncated slab is much greater than both the impact parameter b and v/ω. Otherwise there may be non-negligible contributions from the top and bottom surfaces of the slab as well as from corner regions. The losses will probably in all cases show roughly an exponential decrease in amplitude with increasing impact parameter.

Aloof beam EELS can allow materials analysis to be performed with significantly reduced electron beam damage which occurs primarily through knock-on or radiolysis processes [81]. When the beam is positioned outside the sample, no strong interactions with the nucleus occurs and the knock-on damage mechanism is shut down. The situation for radiolysis is a little more complicated but Eq (1) suggests that the probability for transferring energy E ($=\hbar\omega$), decreases with increasing impact parameter (due to the Bessel function dependence of b). The advantage of aloof beam EELS for lowering radiation damage was first discussed by Walls and Howie [82]. With ultra-high energy resolution EELS, molecular motifs present in materials may be identified by comparison with IR spectroscopy libraries. Combining the aloof beam acquisition mode with vibrational EELS provides a completely new approach for molecular characterization of radiation sensitive materials in the TEM. Rez and co-workers recently demonstrated the similarity between the vibrational EELS and IR spectroscopy from guanine with each showing characteristic peaks associated with C–O, N–H and C–H species [83].

We have also been exploiting this damage free approach to chemical analysis for probing photocatalytic materials for water splitting. Polymeric carbon nitrides (e.g. $C_xN_yH_z$) have recently attracted attention as a possible visible light water splitting system [84]. However, there is considerable variation in the structures and compositions of these materials and it is not clear which form has the highest catalytic activity. The hydrogen content is a critical question in these materials and we have used aloof beam EELS to chemically probe the materials and also determine the band gap [61]. Fig. 4 shows a typical vibrational EELS spectrum recorded in aloof mode from a carbon nitride. The spectrum shows the presence of peaks at ~165 and 184 meV associated with C–N and s-triazine ring modes, respectively, while the peak centered at ~400 meV corresponds to N–H stretches. Fig. 4 also shows the corresponding IR spectrum recorded from the same material. While the energy resolution of the IR is much higher than vibrational EELS, the STEM approach is able to probe local variations in the chemistry. Also the ability to correlate local chemistry with local bandgap measurements provides a powerful combination for developing a fundamental understanding of structure-reactivity relations for these novel photocatalytic materials.

Aloof beam EELS has also been able to detect and differentiate between hydroxide and hydrate species [53]. Fig. 5 shows an aloof beam spectrum from $Ni(NO_3)\cdot 6H_2O$, a typical hydrate. The spectrum is plotted as a function of wavenumber and is compared with the infrared spectrum. The two spectra are very similar and we were also able to show that in the vibrational EELS, H_2O gives rise to a broad peak at 430 meV whereas hydroxide gives a sharper peak at 450 meV.

7. Aloof beam EELS and surface characterization

The original motivation for developing aloof beam EELS was to provide an acquisition mode that was more suitable for exploring the surface response of materials since the bulk spectral contribution was excluded [62,63]. The ability to perform local molecular probing on nanoparticles surfaces to determine both composition and electronic structural information without radiation damage would be highly desirable to fields such as catalysis. Sensing and identifying adsorbates on the surface of nanoparticles is critical for developing structure-reactivity relations. *In situ* transmission electron microscopy and scanning probe microscopy may be the only approaches that allow such interrogation to be carried out at the atomic level [1]. In general, surface atoms have lower coordination than bulk atoms making bond scission more likely to lead to structural and compositional surface changes. Moreover, in

Please cite this article as: P.A. Crozier, Vibrational and valence aloof beam EELS: A potential tool for nondestructive characterization of nanoparticle surfaces, Ultramicroscopy (2017), http://dx.doi.org/10.1016/j.ultramic.2017.03.011

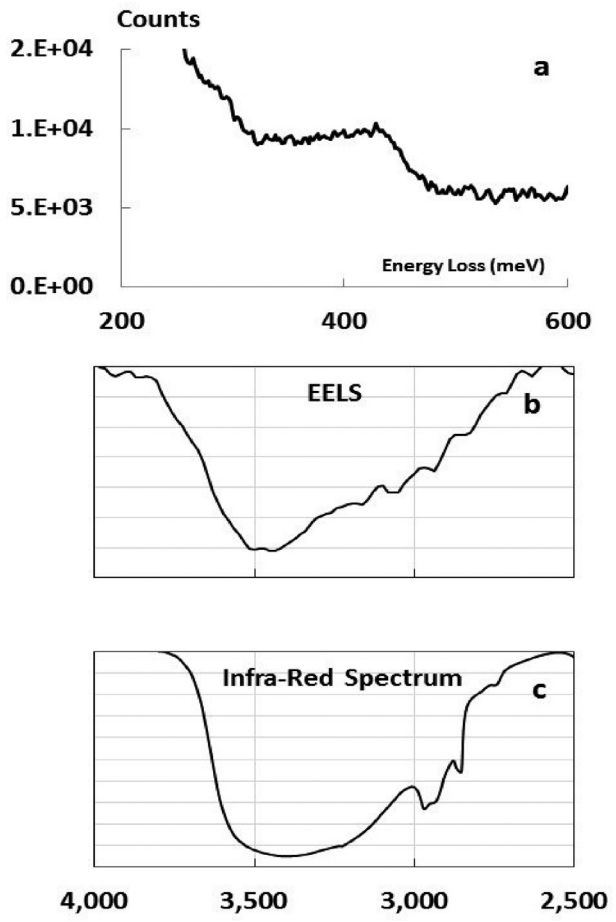

Fig. 5. OH vibrational peak from $Ni(NO_3)_2{\cdot}6H_2O$. **a)** Raw EELS spectrum, **b)** background subtracted and inverted EELS plotted against wavenumber **c)** IR spectrum showing same wavenumber range as (b) (Courtesy of Crozier et al, [53] – with permission Elsevier).

the bulk, kinetic barriers may slow atom diffusion increasing the probability that the bond may reform allowing the structure to repair itself. On surfaces, upon bond scission, atoms may easily desorb into the gas phase leading to rapid changes in surface structure and composition. Thus surfaces undergo radiation damage far more rapidly than bulk structures.

Aloof beam EELS may make it possible to identify surface species without inducing the surface damage associated with transmission techniques. Vibrational EELS is ideal for molecular identification but is not yet available on the current generation of environmental TEMs [1–3]. However, the monochromators available on existing ETEMs allow EELS to be performed under *in situ* conditions at resolutions of around 100 meV. Thus aloof beam valence loss spectroscopy can be performed under reaction conditions. *In situ* monitoring of changes in the aloof beam spectrum may provide information on dynamic changes taking place on the surface of the nanoparticle under reaction conditions.

The simple picture used to derive Eq. (1) assumes that the surface is abruptly terminated and that the dielectric response function is the same throughout. The surface response (the so-called surface plasmons or phonons) simply reflects the boundary condition that arises from the bulk/vacuum interface. In reality, the surface structure will rarely be bulk terminated and for applications in fields such as catalysis, the surface composition will always be different from the bulk. Consequently the sensitivity of the surface EELS response to changes in the composition or structure of the surface layers becomes important. Several authors have considered

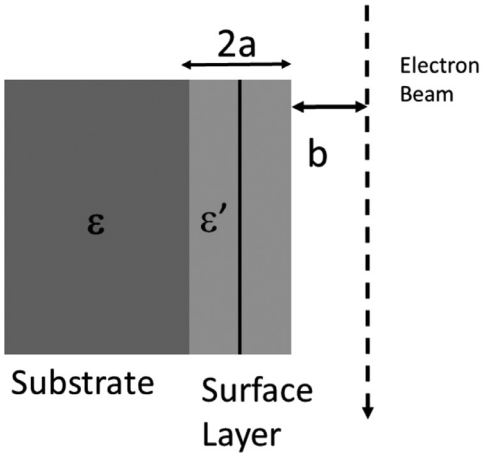

Fig. 6. Geometry for electron passing a thin layer on surface of substrate, dielectric ε and a surface layer of thickness 2a and dielectric ε'. The impact parameter, b, is measured from the top of the surface layer.

geometries that allow coatings to be modelled by including a thin layer with a different dielectric function e.g. [68,85–88]. The non-relativistic coated slab model gives the simplest analytical expression and, assuming that the electron beam is travelling through the vacuum (see Fig. 6), can be written as [86]

$$\frac{d^2P}{dqdE} \propto F\left(\varepsilon, \varepsilon', K, a\right)\exp(-Kb)/Kv^2 \tag{2}$$

with

$$F\left(\varepsilon, \varepsilon', K, a\right) = Im\left\{\frac{\left[\left(\varepsilon'+\varepsilon\right)\left(\varepsilon'-1\right)\exp\left(2Ka\right)-\left(\varepsilon'-\varepsilon\right)\left(\varepsilon'+1\right)\exp\left(-2Ka\right)\right]}{\left[\left(\varepsilon'+\varepsilon\right)\left(\varepsilon'+1\right)\exp\left(2Ka\right)-\left(\varepsilon'-\varepsilon\right)\left(\varepsilon'-1\right)\exp\left(-2Ka\right)\right]}\right\}$$

and

$$K^2 = q^2 + \frac{\omega^2}{v^2}$$

where q is the change in wavevector parallel to the surface. As discussed by Howie and Milne[86], the term F is most sensitive to the surface layers for larger values of K and, for a given energy loss, this can be accomplished by using off-axis geometry or lower electron velocity for spectral collection. (Notice that Eq. (2) shows an exponential dependence on impact parameter b and also contains a q dependence. The Bessel function impact parameter dependence of Eq. (1) arises because ε is assumed to be independent of q and an integral over q has been carried out).

An important question that must be explored concerns the sensitivity of aloof beam EELS for detecting surface layers. The aloof signal is influenced not only by the surface layer but also by the underlying substrate. Certainly nanometer thick oxide layers can be detected but what about a submonolayer molecular film. Eq. (2) provides a simple way to explore this question. Eq. (2) is certainly a "best case" scenario since it does not include Cherenkov or guided light modes. Moreover, it is not clear how far one can push these dielectric models for thin layers especially for submonolayers that are likely to be discontinuous. However, it is a simple starting point and provides at least and initial guide to what to expect at lower accelerating voltages on smaller nanoparticles of lower refractive index (see Section 8). A series of spectral simulations were performed for a 0.2 nm thick layer on a TiO_2 substrate for an incident electron energy, E_o, of 60 kV to illustrate the surface sensitivity with varying q. The thin film is a simple Drude oscillator with a resonance at 2.5 eV, selected to lie within the 3.2 eV bandgap of anatase. The dielectric data for the anatase was an average of

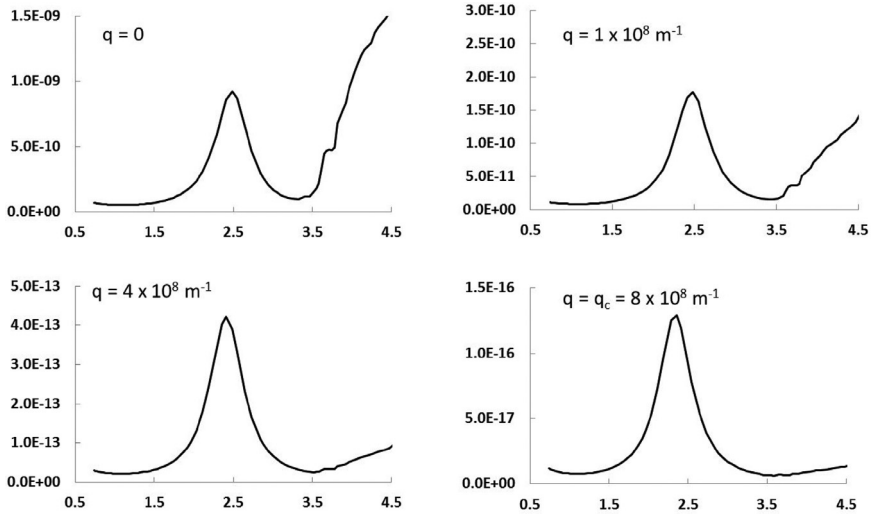

Fig. 7. Simulations of aloof beam EELS spectrum for different values of q for 0.2 nm of Drude oscillator $E_p = 2.5$, on TiO_2 (anatase) substrate. Impact parameter b = 10 nm, $E_o = 60$ kV. Energy-loss in eV along horizontal axes. The vertical axis is in arbitrary units but is proportional to the scattering probability.

the dielectric function parallel and perpendicular to the c-axis [89]. Defining $\theta_E = \Delta E/2E_0$ and assuming a cutoff angle of $\theta c \sim (\theta_E)^{0.5}$ with $q_c = k_o \theta c$ where k_o is the incident wavevector for the fast electron, the form of the spectrum can be calculated for different values of q up to the cutoff value. Fig. 7 shows that the intensity of the peak at 2.5 eV relative to the TiO_2 substrate conduction band edge signal increases dramatically with increasing q showing that the scattering becomes more localized to the surface. However, the absolute intensity of the spectrum also drops by many orders of magnitude as q increases. At the cut-off value, $q_c = 8 \times 10^8$ m^{-1}, the intensity is 7 orders of magnitude lower than the q = 0 case. This is because K appears in the argument of the exponential term involving the impact parameter b in Eq. (2). To maintain the same signal strength as q is increased, the beam must be placed closer to the sample and simulation shows that at the cut-off value of q, the impact parameter is only 0.1 nm. Thus to get the highest surface sensitivity, the electron beam is effectively touching the sample surface and radiation damage will be correspondingly increased. Moreover, from a practical point of view, such small impact parameters are unrealistic for aloof beam EELS because of the incident-beam convergence.

For damage free surface analysis, the optimum scattering angle may be one that maximizes surface sensitivity and minimizes damage. In practice, the STEM geometry typically involves a probe convergence semi-angle of 10 – 30 mrad and an EELS collection semi-angle up to 50 mrad. Thus each spectrum is an average over a range of q although the intensity will be heavily weighted by the low q contributions. In future spectrometers, it may be possible to use annular entrance apertures to increase the intensity of the higher angle scattering. However, to evaluate the potential benefits of such a cylindrical collection geometry on surface analysis, Eq. (2) cannot be employed since the change in wavevector, q, is only the component parallel to the surface. Also the q dependence of the dielectric response functions should be explicitly included in the calculation.

For oxide catalysts, the substrate is an insulator and the signal associated with adsorbates or electronic defects may give rise to spectral intensity within the bandgap region. In favorable cases, the spectral intensity in the bandgap region from the substrate may be very small, increasing the sensitivity for detecting the surface layer even for the forward scattering geometry. To explore this behavior, aloof beam spectra have been simulated for a layer of TiO_2 (bandgap 3.2 eV) on an MgO substrate, bandgap 7.3 eV Fig. 8a shows that even for a 0.1 nm surface layer, the TiO_2 signal is easily detectable within the bandgap of the MgO. Indeed in the spectral region more than 1 eV below the MgO band edge, the TiO_2 surface signal looks very similar to the bulk TiO_2 with only a slight shift in the peak positions as shown in Fig. 8b. (Of course in a real sample, it is unlikely that such a thin TiO_2 layer could be accurately represented by a bulk dielectric function but this approach provides order of magnitude estimates of the signal strength from the thin layer). The TiO_2 signal initially increases approximately linearly with increasing layer thickness and the MgO signal drops. When the TiO_2 thickness is 5 nm, the MgO signal is very weak and the spectrum has converged to the aloof beam spectrum from a bulk terminated TiO_2 surface.

Detecting surface signals (either vibrational or bandgap electronic states) is certainly feasible on insulators or semiconductors if relativistic effects are small because the substrate intensity in the bandgap is very low. The situation for a metal substrate is more challenging because the weak surface signal will sit on a large electronic excitation background. This situation was simulated for layers of TiO_2 (anatase) on a drude metal substrate with a resonance at 20 eV and width of 5 eV The result is plotted in Fig. 9 and shows that the thinnest layer of TiO_2 (0.1 nm) is barely visible on the large background from the metal. At a thickness of 1 nm, the TiO_2 signal becomes easily detectable above the metal background.

To test the experimental ability to perform surface nanoanalysis of thin, radiation sensitive layers, we recently conducted experiments on MgO nanocubes with a surface hydrate layer [90]. MgO and $Mg(OH)_2$ have refractive indices (in the bandgap region) of 1.8 and 1.3 respectively making relativistic effects small. The transmission and aloof beam spectra recorded with the Nion monochromated system are reproduced in Fig. 10 and the aloof beam spectrum shows intensity within the bandgap region that we associate with the hydrated layer. Simulations using Eq. (2) showed a good fit indicating that a thin hydrated layer was present. (More accurate relativistic calculations will be published later which also support the current interpretation). This supports the conclusion that local surface analysis without radiation damage is feasible with the aloof beam approach. Comparing Figs. 10 and 8c shows that the sensitivity for detecting the magnesium hydroxide is considerably poorer than the TiO_2 simulation suggests. The strength of the spectroscopic signal from the thin layer is primarily controlled by the imaginary part of the dielectric function which, for the hydroxide, is an order of magnitude smaller than the TiO_2 case.

Please cite this article as: P.A. Crozier, Vibrational and valence aloof beam EELS: A potential tool for nondestructive characterization of nanoparticle surfaces, Ultramicroscopy (2017), http://dx.doi.org/10.1016/j.ultramic.2017.03.011

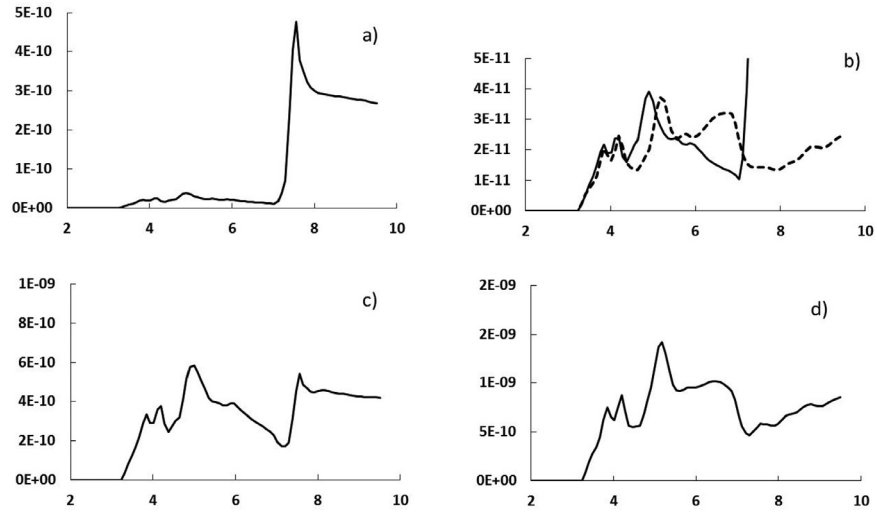

Fig. 8. Simulations of aloof beam EELS spectrum based on Eq. (2) for thin layer of TiO_2 on MgO substrate. **a)** and **b)** 0.1 nm TiO_2 with **b)** also showing aloof spectra from TiO_2 layer and scaled TiO_2 bulk terminated surface (dotted) **c)** 1 nm and **d)** 5 nm. Impact parameter b = 10 nm, E_o = 60 kV, energy loss in eV along horizontal axis.

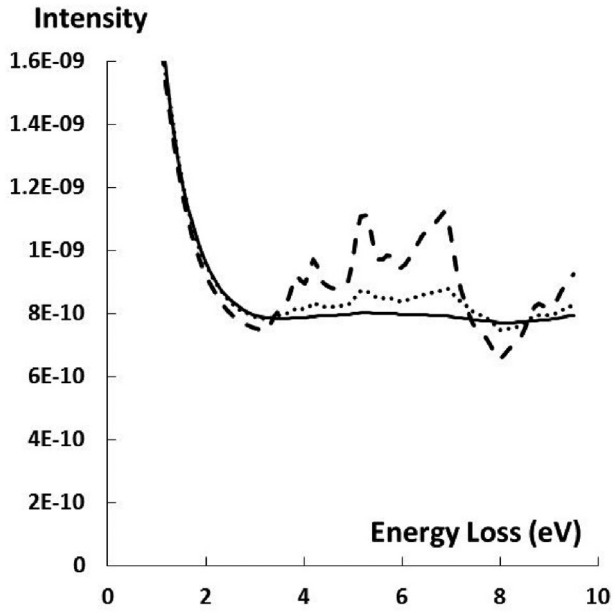

Fig. 9. Simulations of aloof beam EELS spectrum for thin layers of TiO_2 on Drude metal (E_p = 20 eV, Γ = 5 eV). Impact parameter b = 10 nm, E_o = 60 kV. TiO_2 layer is 0.1 nm (solid), 1 nm (dotted) and 5 nm (dashed).

The aloof beam vibrational EELS approach was also tested on the same MgO sample described above[53]. The spectrum in Fig. 11 shows the presence of a broad peak centered at 430 meV. For OH species, hydroxides give a sharp peak at 450 meV and hydrates give a broad peak at 430 meV. The spectrum from the MgO surface looks similar to the hydrate spectrum shown in Fig. 5 suggesting that the surface layer on the MgO cube is a hydrate layer not a hydroxide layer. This demonstrated an advantage of the vibrational approach compared to the valence loss method in that the spectral finger print can be interpreted directly in terms of a molecular motif.

8. Complications: relativistic and particle size effects

It is well known that relativistic effects complicate the interpretation of the aloof beam spectrum at higher electron beam energies. Cherenkov emission and other retardation effects associated with large impact parameters can result in large deviations from the spectral form predicted by Eq. (2). One consequence for the insulating oxides considered here, is that the spectral intensity within the bandgap region becomes a function of both the real and imaginary parts of the dielectric functions. Cherenkov radiation is a relativistic effect that arises when the electron, or in the aloof beam case, the image charge, travels faster than the speed of light in the medium. In this case, a necessary condition for the genera-

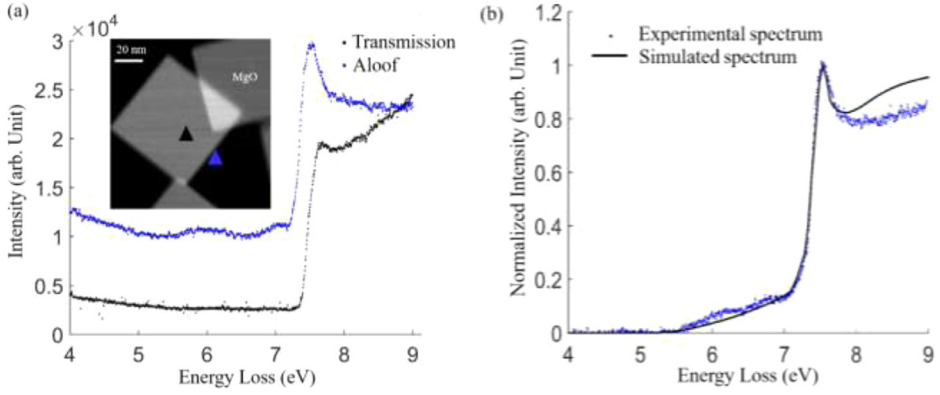

Fig. 10. a) The transmission (black) and aloof beam spectrum (blue) from the (100) surface of MgO cube exposed to water vapor (E_o = 60 kV). **b)** Background subtracted aloof spectrum from a) and simulated spectrum (black) using Eq. (2) assuming 1.5 nm layer of magnesium hydroxide is present. (Courtesy of Liu et al, [90]– with permission Elsevier). (For interpretation of the references to colour in this figure legend, the reader is referred to the web version of this article.)

Please cite this article as: P.A. Crozier, Vibrational and valence aloof beam EELS: A potential tool for nondestructive characterization of nanoparticle surfaces, Ultramicroscopy (2017), http://dx.doi.org/10.1016/j.ultramic.2017.03.011

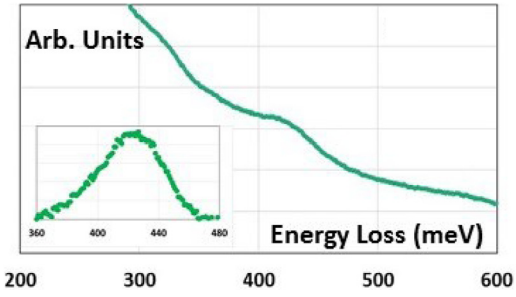

Fig. 11. Aloof-mode vibrational spectrum from surface of same MgO cube of Fig. 10. The OH stretch at 430 meV associated with surface OH layer (the insert shows the vibrational peak after background subtraction). (Courtesy of Crozier et al, [53]– with permission).

tion of Cherenkov is that, $v > c/n$ where n is the refractive index for the energy-loss of interest, v is the velocity of the fast electron and c is the speed of light in the vacuum. Thus low refractive index materials are less likely to show Cherenkov effects in EELS at lower accelerating voltages.

The Cherenkov threshold condition does not provide any information on the strength of the Cherenkov signal in the spectrum. For example, it is well known that particle size strongly influences the effect of Cherenkov radiation on the spectrum. For particles sizes that are substantially smaller than the wavelength of the emitted photons, the Cherenkov effect is suppressed [33,35]. Other retardation effects, such as the time it takes the fast electron signal to reach the surface have been discussed by Rivacoba and will be present regardless of refractive index [74]. These effects will increase with increasing impact parameter so this may be an argument for keeping the impact parameter as small as radiation damage will allow. In less favorable cases, it may not be easy to differentiate the bandgap intensity due to relativistic effects from weak signals associated with the presence of surface states without extensive simulation. Even if such a differentiation is achieved, the additional intensity generated in the bandgap by relativistic effects will decrease the detection limits for surface states.

The critical refractive index above which Cherenkov effects are likely to become important is plotted as a function of accelerating voltage in Fig. 12a. The refractive indices (at 589 nm) of oxides supports commonly employed in heterogeneous catalysts is also shown on the graph [91]. The graph shows that significant relativistic effects will be present in all materials at higher accelerating voltages (i.e. 200 kV). Supports such as MgO, SiO_2 and Al_2O_3 have refractive indices of 1.75 or less and Cherenkov effects should be small at accelerating voltages of 100 kV or lower. TiO_2 has a significantly higher refractive index (2.4 – 2.6) and accelerating voltages of 20 - 40 kV may lead to simpler spectral interpretations. One advantage of the aloof beam approach compared to transmission EELS is that the scattering probability is rather small so lower accelerating voltages do not give large multiple scattering effects. For constant impact parameter b, the exponential and Bessel function terms involving b and v (see Eqs. (1) and (2)), shows that the intensity of the spectrum will drop because of the reduction in v so smaller impact parameters may be required for adequate signal-to-noise.

For applications to catalysts, the sample is in the form of a particle not an infinite half plane. For this case a spherical geometry is more appropriate and there have been several analyses using Mie type treatments of the electron scattering problem [73,80,92,93]. With the spherical geometry it is possible for the electric field associated with the fast electron to couple with the electromagnetic cavity modes of the particle leading to standing waves or so-called guided light modes. These guided light modes can give rise to oscillatory spectral intensity within the bandgap region which may obscure weaker features associated with changes in surface structure. The resonant modes may be predicted for arbitrary geometries using classical electrodynamic models as demonstrated for GaN nanowires [94]. The position of the maxima and minima is determined by the geometry of the particle and the lowest peak in the energy-loss spectrum will arise from the resonance mode associated with the largest wavelength.

Full numerical simulation can accurately predict the location of these spectral features in oxide nanoparticle [95]. A simple 1D analysis can also provide an approximate estimate of when guided light modes may give rise to intensity within the bandgap region. The energy of a resonant standing light wave for a 1D particle of dimension L can be expressed as

$$E = hmc/2nL \quad (3)$$

where n is the refractive index and m is the order. The lowest energy mode ($m = 1$) is plotted in Fig. 12b for typical refractive indices for oxide supports. This shows that the energy of the lowest mode decreases with increasing particle size and refractive index. The exact position of the peak will depend on the particle geometry and other factors such as the degree to which the standing photon wave spills into the vacuum. Also the strength of the oscillations will depend on the degree of coupling between the fast electron and the resonant modes as well as the damping in the material. However, for detection of electronic states within the bandgap, Fig. 12b can be used to roughly estimate how small the particle should be to avoid having oscillations within the bandgap region. For an oxide like TiO_2, with refractive index of 2.5 and

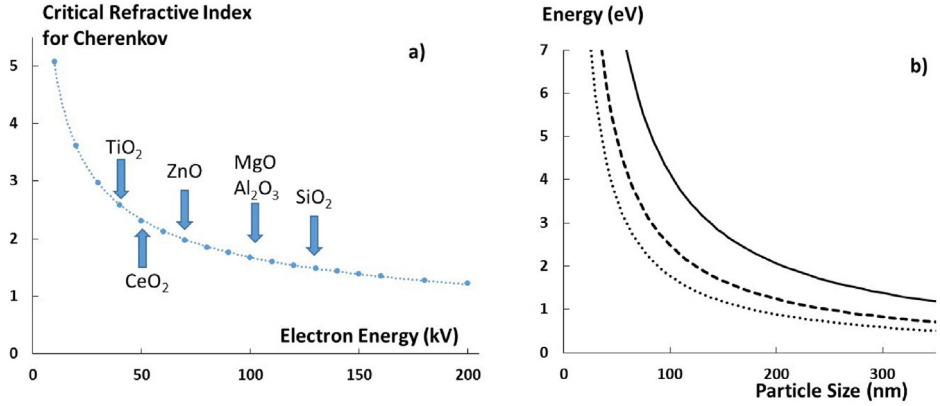

Fig. 12. a) Critical refractive index for Cherenkov condition versus electron beam energy. **b)** Approximate lowest energy optical cavity mode as a function of particle size for refractive indices of 1.5 (solid), 2.5 (dashed) and 3.5 (dotted).

bandgap of 3.3 eV, we would not expect to see guided mode maxima or minima in the bandgap region for particles less than 75 nm. In smaller particles, this energy-loss mechanism will contribute a slowly varying background within the bandgap region negatively impacting the detection limits for surface structure. Our experience with materials like TiO_2, suggests that for spectra recorded at 60 and 100 kV, peaks are present in the bandgap region which depend sensitively on particle size/shape and may be significantly enhanced at higher accelerating voltage [90]. For vibrational EELS, the particle size needs to be greater than 400 nm to see peaks in the vibrational energy range (450 meV or below).

9. Looking ahead and closing remarks

The technique of aloof beam EELS in a monochromated STEM shows promise for surface characterization while minimizing electron beam induced damage. The vibrational signal is similar to infrared spectroscopy and can provide molecular identification as well as information on phonon modes. The valence-loss signal can also provide information on composition and the dielectric response in the visible region. The initial results on insulating oxide substrates show that, at lower accelerating voltage, the bandgap provides a low background spectroscopic window to sense the presence of surface layers. Both the vibrational and electronic signal in the bandgap region are weak and would benefit with improved detection efficiency. The sensitivity is most favorable when the imaginary part of the dielectric function of the surface layer is large in the energy-loss region of the bandgap substrate. The surface sensitivity of aloof beam EELS acquired in the conventional forward scattering geometry is limited. The ability to collect a significant fraction of the higher angle scattering through some sort of annular collection geometry without degrading spectral resolution would increase the surface to bulk signal ratio. Surface sensitivity is also improved by using lower accelerating voltage. Continued detector system improvements in both detection quantum efficiency and modulation transfer function which reduces the tails on the zero-loss signal would provide greater detection of the vibrational fingerprints of surface adsorbates.

Guided light modes may complicate the interpretation of the intensity in the bandgap region. For the common oxide supports of relevance to catalysis, these effects seem to be considerably reduced for particle sizes less than 75 nm although spectral simulation should be performed especially for systems with larger refractive indices in the spectral region of interest. Cherenkov and other retardation effects can also be problematic particularly for systems of higher refractive index. For oxide systems, the refractive index in the bandgap region rarely exceeds 3 and working at accelerating voltages of 20 – 40 kV should help to minimize the relativistic effects assuming the impact parameter is small (< 5 nm). Spectral simulations are important to ensure correct interpretation especially for the valence loss region. For areas such as catalysis, detecting the changes in the aloof beam spectra that occur with changes in temperature and gas composition will provide a potentially new tool for determining structure-reactivity relations. Thus to realize the full potential of this advanced spectroscopy capability, it must be made available for *in situ* or *operando* microscope configurations.

Acknowledgements

I would like to thank Ondrej Krivanek and Nion for their tireless effort on instrument development. I am grateful to Archie Howie (Department of Physics, Cambridge University) and my colleague Peter Rez here at ASU for many enlightening discussions. Thanks also go to David Masiello and Steven Quillin at the University of Washington for helpful discussions and detailed relativistic calculations on guided light modes. I must also acknowledge the contributions of my Ph.D. students especially Qianlang Liu, Will Bowman and Diane Haiber. The financial support from US Department of Energy (DE-SC0004954) and the use of NION UltraSTEM at John M. Cowley Center for High Resolution Microscopy at Arizona State University are gratefully acknowledged.

References

[1] F. Tao, P.A. Crozier, Atomic-scale observations of catalyst structures under reaction conditions and during catalysis, Chem. Rev. 116 (6) (2016) 3487–3539.
[2] P.A. Crozier, B.K. Miller, Spectroscopy of solids, gases and liquids in the ETEM, in: T.W. Hansen, J.B. Wagner (Eds.), Controlled Atmosphere Transmission Electron Microscopy, Springer, New York, 2015.
[3] P.A. Crozier, T.W. Hansen, In situ and operando transmission electron microscopy of catalytic materials, MRS Bull. 40 (01) (2015) 38–45.
[4] M.A. Bañares, I.E. Wachs, Molecular structures of supported metal oxide catalysts under different environments, J. Raman Spectroscopy 33 (2002) 359.
[5] A.V. Crewe, Scanning electron microscopes: is high resolution possible? Science 154 (3750) (1966) 729–738.
[6] A.V. Crewe, M. Isaacson, D. Johnson, Electron energy loss spectra of nucleic acid bases, Nature 231 (5300) (1971) 262–&.
[7] M. Isaacson, Interaction of 25 keV electrons with the nucleic acid bases, adenine, thymine, and uracil. II. Inner shell excitation and inelastic scattering cross sections, J. Chem. Phys. 56 (5) (1972) 1813–1818.
[8] M. Isaacson, D. Johnson, Microanalysis of light-elements using transmitted energy-loss electrons, Ultramicroscopy 1 (1) (1975) 33–52.
[9] A. Howie, O.L. Krivanek, M.L. Rudee, Interpretation of electron micrographs and diffraction patterns of amorphous materials, Philosoph. Mag. 27 (1) (1973) 235–255.
[10] O.L. Krivanek, Influence of beam intensity on electron-microscope contrast transfer-function, Optik 43 (4) (1975) 361–372.
[11] O.L. Krivanek, A. Howie, Kinematical theory of images from polycrystalline and random-network structures, J. Appl. Crystallography 8 (APR1) (1975) 213–219.
[12] O.L. Krivanek, S. Isoda, K. Kobayashi, Lattice imaging of a grain-boundary in crystalline germanium, Philosoph. Mag. 36 (4) (1977) 931–940.
[13] O.L. Krivanek, et al., Electron energy loss spectroscopy as a probe of the local atomic environment, Ultramicroscopy 9 (3) (1982) 249–254.
[14] O. Krivanek, Imaging and microanalysis with high spatial-resolution, castle-hot-springs, Ultramicroscopy 9 (3) (1982) 179–180.
[15] O.L. Krivanek, P.R. Swann, An advanced electron energy-loss spectrometer, in: G.W. Lorimer, M.H. Jacobs, P. Doig (Eds.), Quantitative Microanalysis with High Spatial Resolution, The Metals Society, Manchester, 1981, pp. 136–140.
[16] O.L. Krivanek, C.C. Ahn, R.B. Keeney, Parallel detection electron spectrometer using quadrupole lenses, Ultramicroscopy 22 (1-4) (1987) 103–115.
[17] O.L. Krivanek, et al., Design and 1st applications of a postcolumn imaging filter, Microscopy Microanaly. Microstruct. 3 (2-3) (1992) 187–199.
[18] P.E. Batson, High-energy resolution electron spectrometer for 1-nm spatial analysis, Rev. Sci. Instrum. 57 (1) (1986) 43–48.
[19] R. Brydson, et al., Electron energy-loss and x-ray absorption spectroscopy of rutile and anatase - a test of structural sensitivity, J. Phys. 1 (4) (1989) 797–812.
[20] W. Engel, et al., Electron energy-loss spectroscopy and the crystal chemistry of rhodizite. Part 1.-Instrumentation and chemical analysis, J. Chem. Soc. Faraday Trans. 1 84 (2) (1988) 617–629.
[21] O.L. Krivanek, J.H. Paterson, ELNES of 3d transition-metal oxided. 1. Variation across the periodic table, Ultramicroscopy 32 (4) (1990) 313–318.
[22] J.H. Paterson, O.L. Krivanek, ELNES of 3d transition-metal oxided. 1. Variation with oxidation state and crystal structure, Ultramicroscopy 32 (4) (1990) 319–325.
[23] M. Terauchi, et al., Performance of a new high-resolution electron energy-loss spectroscopy microscope, Microscopy Microanaly. Microstruct. 2 (2-3) (1991) 351–358.
[24] H.W. Mook, P. Kruit, On the monochromatisation of high brightness electron sources for electron microscopy, Ultramicroscopy 78 (1-4) (1999) 43–51.
[25] P.C. Tiemeijer, Operation modes of a TEM monochromator, in: C.J. Kiely (Ed.), Electron Microscopy and Analysis 1999, Iop Publishing Ltd, Bristol, 1999, pp. 191–194.
[26] H. Rose, Electrostatic energy filter as monochromator of a highly coherent electron source, Optik 86 (3) (1990) 95–98.
[27] C. Mitterbauer, et al., Electron energy-loss near-edge structures of 3d transition metal oxides recorded at high-energy resolution, Ultramicroscopy 96 (3-4) (2003) 469–480.
[28] M.O. Krause, J.H. Oliver, Natural widths of atomic K and L levels, Kα X-ray lines and several KLL Auger lines, J. Phys. Chem. Reference Data 8 (2) (1979) 329–338.
[29] S. Lazar, et al., Materials science applications of hreels in near edge structure analysis and low-energy loss spectroscopy, Ultramicroscopy 96 (2003) 535–546.
[30] M. Stoger-Pollach, et al., Cerenkov losses: a limit for bandgap determination and Kramers-Kronig analysis, Micron 37 (2006) 396–402.
[31] M. Bosman, et al., Mapping surface plasmons at the nanometer scale with an electron beam, Nanotechnology 18 (2007) 165505.

Please cite this article as: P.A. Crozier, Vibrational and valence aloof beam EELS: A potential tool for nondestructive characterization of nanoparticle surfaces, Ultramicroscopy (2017), http://dx.doi.org/10.1016/j.ultramic.2017.03.011

[32] J. Nelayah, et al., Mapping surface plasmons on a single metallic nanoparticle, Nat. Phys. 3 (5) (2007) 348–353.
[33] R. Erni, N.D. Browning, The impact of surface and retardation losses on valence electron energy-loss spectroscopy, Ultramicroscopy 108 (2) (2008) 84–99.
[34] R. Erni, S. Lazar, N.D. Browning, Prospects for analyzing the electronic properties in nanoscale systems by VEELS, Ultramicroscopy 108 (2008) 270–276.
[35] M. Stoger-Pollach, Optical properties and bandgaps from low loss EELS: pitfalls and solutions, Micron 39 (2008) 1092–1110.
[36] M. Stoger-Pollach, A. Laister, P. Schattschneider, Treating retardation effects in valence EELS spectra for Kramers-Kronig analysis, Ultramicroscopy 108 (2008) 439–444.
[37] D.T.L. Alexander, P.A. Crozier, J.R. Anderson, Brown carbon spheres in east asian outflow and their optical properties, Science 321 (5890) (2008) 833–836.
[38] J.T. Zhu, et al., Derivation of optical properties of carbonaceous aerosols by monochromated electron energy-loss spectroscopy, Microscopy Microanal. 20 (3) (2014) 748–759.
[39] L.K. Ondrej, et al., High-energy-resolution monochromator for aberration-corrected scanning transmission electron microscopy/electron energy-loss spectroscopy, Philosoph. Trans. A 367 (1903) (2009) 3683–3697.
[40] J.P. Perez, et al., 1st-order study of a dispersive, magnetic, symmetrical alpha–type system, J. De Physique 45 (NC-2) (1984) 171–174.
[41] O.L. Krivanek, et al., Monochromated STEM with a 30 meV-wide, atom-sized electron probe, Microscopy 62 (1) (2013) 3–21.
[42] P. Rez, Is localized infrared spectroscopy now possible in the electron microscope? Microscopy Microanal. 20 (03) (2014) 671–677.
[43] R.F. Egerton, Prospects for vibrational-mode EELS with high spatial resolution, Microscopy Microanal. 20 (03) (2014) 658–663.
[44] O.L. Krivanek, et al., Vibrational spectroscopy in the electron microscope, Nature 514 (2014) 209–212.
[45] T. Miyata, et al., Measurement of vibrational spectrum of liquid using monochromated scanning transmission electron microscopy-electron energy loss spectroscopy, Microscopy 63 (5) (2014) 377–382.
[46] M.J. Lagos, P.E. Batson, Mapping EELS vibrational modes in MgO nanocubes, Microscopy Microanal. 22 (S3) (2016) 954–955.
[47] W.J. Bowman, et al., Measuring bandgap states in individual non-stoichiometric oxide nanoparticles using monochromated STEM EELS: the Praseodymium–ceria case, Ultramicroscopy 167 (2016) 5–10.
[48] R.F. Egerton, Electron Energy-Loss Spectroscopy in the Electron Microscope, Third ed., Plenum Press, New York, NY, 2011, pp. 255–262.
[49] B.D. Forbes, L.J. Allen, Modeling energy-loss spectra due to phonon excitation, Phys. Rev. B 94 (2016).
[50] R.F. Egerton, Vibrational-loss EELS and the avoidance of radiation damage, Ultramicroscopy 159 (Part 1) (2015) 95–100.
[51] C. Dwyer, Localization of high-energy electron scattering from atomic vibrations, Phys. Rev. B 89 (5) (2014) 5.
[52] P. Cueva, D.A. Muller, Atomic-scale optical and vibrational spectroscopy with low loss EELS, Microsc. Microanal. 19 (Suppl 2) (2013) 1130–1131.
[53] P.A. Crozier, T. Aoki, Q. Liu, Detection of water and its derivatives on individual nanoparticles using vibrational electron energy-loss spectroscopy, Ultramicroscopy 169 (2016) 30–36.
[54] K. Venkatraman, et al., Investigating the spatial resolution of vibrational electron energy-loss spectroscopy, Microscopy Microanal. 22 (Suppl. (3)) (2016) 992–993.
[55] S.J. Pennycook, P.D. Nellist (Eds.), Scanning Transmission Electron Microscopy, Springer, New York, 2011.
[56] H. Ibach, D.L. Mills, Electron Energy Loss Spectroscopy and Surface Vibrations, Academic Press, 1982.
[57] F. Lu, M.Z. Jin, M.A. Belkin, Tip-enhanced infrared nanospectroscopy via molecular expansion force detection, Nat. Photon. 8 (4) (2014) 307–312.
[58] J.R. Felts, et al., Atomic force microscope infrared spectroscopy on 15 nm scale polymer nanostructures, Rev. Sci. Instrum. 84 (2) (2013) 6.
[59] A. Dazzi, et al., AFM-IR: combining atomic force microscopy and infrared spectroscopy for nanoscale chemical characterization, Appl. Spectroscopy 66 (12) (2012) 1365–1384.
[60] C. Dwyer, et al., Electron-beam mapping of vibrational modes with nanometer spatial resolution, Phys. Rev. Lett. 117 (25) (2016).
[61] D. Haiber, T. Aoki, P.A. Crozier, Exploring vibrational and electronic structure of carbon nitride powders using monochromated electron energy-loss spectroscopy, Microscopy Microanal. 22 (3) (2016) 986–987.
[62] Y. Ballu, J. Lecante, D.M. Newns, Surface plasmons on Mo (100), Phys. Lett. A 57 (2) (1976) 159–160.
[63] J. Lecante, Y. Ballu, D.M. Newns, Electron-surface-plasmon scattering using a parabolic non-touching trajectory, Phys. Rev. Lett. 38 (1) (1977) 36–40.
[64] P.E. Batson, M.M.J. Treacy, Low energy-loss structure of small aluminum particles, in: G.W. Bailey (Ed.), Proceedings of the 38th Annual Meeting of the Electron Micrsocopy Society of America, Claitor's Publishing Division, Baton Rouge: Reno, 1980, pp. 126–127.
[65] P.E. Batson, A new surface plasmon resonance in clusters of small aluminum spheres, Ultramicroscopy 9 (3) (1982) 277–282.
[66] P.E. Batson, Surface plasmon coupling in clusters of small spheres, Phys. Rev. Lett. 49 (13) (1982) 936–940.
[67] L.D. Marks, Observation of the image force for fast electrons near an MgO surface, Solid State Commun. 43 (10) (1982) 727–729.
[68] P.E. Batson, Surface plasmon scattering on flat surfaces at grazing incidence, Ultramicroscopy 11 (4) (1983) 299–302.
[69] J.M. Cowley, Energy losses of fast electrons at crystal surfaces, Phys. Rev. B 25 (2) (1982) 1401–1404.
[70] J.M. Cowley, Surface energies and surface structure of small crystals studied by use of a stem instrument, Surf. Sc. 114 (2) (1982) 587–606.
[71] R.J. Warmack, et al., Surface-plasmon excitation during aloof scattering of low-energy electrons in micropores in a thin metal foil, Phys. Rev. B 29 (8) (1984) 4375–4381.
[72] R. García-Molina, et al., Retardation effects in the interaction of charged particle beams with bounded condensed media, J. Phys. C 18 (1985) 5335–5345.
[73] Z.L. Wang, Valence electron excitations and plasmon oscillations in thin films, surfaces, interfaces and small particles, Micron 27 (1996) 265–299.
[74] A. Rivacoba, N. Zabala, J. Aizpurua, Image potential in scanning transmission electron microscopy, Progress Surf. Sci. 65 (1–2) (2000) 1–64.
[75] F.J.G. de Abajo, Optical excitations in electron microscopy, Rev. Modern Phys. 82 (1) (2010) 209–275.
[76] P.M. Echenique, J.B. Pendry, Absorption profile at surfaces, J. Phys. C 8 (18) (1975) 2936–2942.
[77] A. Howie, Surface-reactions and excitations, Ultramicroscopy 11 (2-3) (1983) 141–148.
[78] C.A. Walsh, An analytical expression for the energy-loss of fast electrons traveling parallel to the Axid of a cylindrical interface, Philosoph. Mag. B 63 (5) (1991) 1063–1078.
[79] N. Zabala, A. Rivacoba, P.M. Echenique, Energy-loss of electrons travelling through cylindrical holes, Surf. Sci. 209 (3) (1989) 465–480.
[80] P.M. Echenique, A. Howie, D.J. Wheatley, Excitation of dielectric spheres by external electron-beams, Philosoph. Mag. B 56 (3) (1987) 335–349.
[81] L.W. Hobbs, Radiation effects in analysis of inorganic specimens by TEM, in: J.J. Hren, J.I. Goldstein, D.C. Joy (Eds.), Introduction to Analytical ELectron Microscopy, Springer, US, 1979, pp. 437–480.
[82] M.G. Walls, A. Howie, Dielectric theory of localized valence energy-loss spectroscopy, Ultramicroscopy 28 (1-4) (1989) 40–42.
[83] P. Rez, et al., Damage-free vibrational spectroscopy of biological materials in the electron microscope, Nat. Commun. 7 (2016) 7.
[84] J. Liu, et al., Metal-free efficient photocatalyst for stable visible water splitting via a two-electron pathway, Science 347 (6225) (2015) 970–974.
[85] P. Moreau, et al., Relativistic effects in electron-energy-loss-spectroscopy observations of the Si/SiO2 interface plasmon peak, Phys. Rev. B 56 (11) (1997) 6774–6781.
[86] A. Howie, R.H. Milne, Excitations at interfaces and small particles, Ultramicroscopy 18 (1985) 427–434.
[87] J.P.R. Bolton, M. Chen, Electron energy loss in multilayered slabs, Ultramicroscopy 60 (2) (1995) 247–263.
[88] M. Couillard, A. Yurtsever, D.A. Muller, *Competition between bulk and interface plasmonic modes in valence electron energy-loss spectroscopy of ultrathin* SiO_2 *gate stacks*, Phys. Rev. B 77 (2008) 085318.
[89] M. Landsmann, E. Rauls, W.G. Schmidt, The electronic structure and optical response of rutile. anatase and brookite TiO2, J. Phys. 24 (2012) 195503.
[90] Q. Liu, K. March, P.A. Crozier, Nanoscale probing of bandgap states on oxide particles using electron energy-loss spectroscopy, Ultramicroscopy (2016) in press.
[91] R.D. Shannon, et al., Refractive index and dispersion of fluorides and oxides, J. Phys. Chem. Reference Data 31 (4) (2002) 931–970.
[92] F.J. Garcia de Abajo, Relativistic energy loss and induced photon emission in the interaction of a dielectric sphere with an external electron beam, Phys. Rev. B 59 (4) (1999) 3095–3107.
[93] D. Ugarte, C. Colliex, P. Trebbia, Surface-plasmon and interface-plasmon modes on small semiconducting spheres, Phys. Rev. B 45 (8) (1992) 4332–4343.
[94] I. Arslan, et al., Using electrons as a high-resolution probe of optical modes in individual nanowires, Nano Lett. 9 (12) (2009) 4073–4077.
[95] L. Q., et al., Understanding guided light modes in oxide nanoparticles with monochromated EELS, Microscopy Microanal. (2017) in press.

Please cite this article as: P.A. Crozier, Vibrational and valence aloof beam EELS: A potential tool for nondestructive characterization of nanoparticle surfaces, Ultramicroscopy (2017), http://dx.doi.org/10.1016/j.ultramic.2017.03.011